# Facilitated Ion Transport in All-Solid-State Flexible Supercapacitors

**Bong Gill Choi,[†] Jinkee Hong,[‡] Won Hi Hong,[†] Paula T. Hammond,[‡,*] and HoSeok Park[§,*]**

[†]Department of Chemical & Biomolecular Engineering (BK21 program), KAIST, Daejeon 305-701, Republic of Korea, [‡]Department of Chemical Engineering, Massachusetts Institute of Technology, Cambridge, Massachusetts 02139, United States, and [§]Department of Chemical Engineering, College of Engineering, Kyung Hee University, 1 Seocheon-dong, Giheung-gu, Yongin-si, Gyeonggi-do 446-701, Republic of Korea

**ABSTRACT** The realization of highly flexible and all-solid-state energy-storage devices strongly depends on both the electrical properties and mechanical integrity of the constitutive materials and the controlled assembly of electrode and solid electrolyte. Herein we report the preparation of all-solid-state flexible supercapacitors (SCs) through the easy assembly of functionalized reduced graphene oxide (f-RGO) thin films (as electrode) and solvent-cast Nafion electrolyte membranes (as electrolyte and separator). In particular, the f-RGO-based SCs (f-RGO-SCs) showed a 2-fold higher specific capacitance (118.5 F/g at 1 A/g) and rate capability (90% retention at 30 A/g) compared to those of all-solid-state graphene SCs (62.3 F/g at 1A/g and 48% retention at 30 A/g). As proven by the 4-fold faster relaxation of the f-RGO-SCs than that of the RGO-SCs and more capacitive behavior of the former at the low-frequency region, these results were attributed to the facilitated ionic transport at the electrical double layer by means of the interfacial engineering of RGO by Nafion. Moreover, the superiority of all-solid-state flexible f-RGO-SCs was demonstrated by the good performance durability under the 1000 cycles of charging and discharging due to the mechanical integrity as a consequence of the interconnected networking structures. Therefore, this research provides new insight into the rational design and fabrication of all-solid-state flexible energy-storage devices as well as the fundamental understanding of ion and charge transport at the interface.

**KEYWORDS:** energy storage · flexible devices · nanostructure · functionalized graphene · Nafion electrolyte

Flexible energy and display devices are of great interest for a wide range of emerging applications in wearable electronics, electronic newspapers, paper-like mobile phones, and other easily collapsible gadgets.[1−6] The realization of high-performance flexible devices strongly depends on the electrical properties and mechanical integrity of the constitutive materials and their controlled assembly into functional devices.[1−6] Recent advances in flexible and miniature devices have been driven by highly conductive robust materials such as flexible carbon nanotube (CNT) thin films, buckling thin metals, stretchable transparent graphene electrodes, and elastic bucky gels.[7−10] Despite these intensive efforts on the design and fabrication of numerous flexible or bendable devices, high-performance flexible energy-storage devices, which should be solid state, compact, sustainable, mobile, and robust over periods of time, are still challenging for the development of the key enabling technologies such as portable and military systems.[11−17]

Among various power source devices, the supercapacitor (SC), a circuit component that can temporarily store a large amount of electrical energy and release it when needed, has been recognized as a future portable energy-storage device due to its high power density and long cycle lifetime, compared with lithium-ion batteries and conventional capacitors.[18−25] In particular, electrical double layer capacitors (EDLCs) have received significant attention owing to the feasibility of easy assembly into an all-solid-state power source that can be sustainable, light, and flexible for emerging applications in mobile and portable devices.[20] The electrode materials hold the key to fundamental approaches and practical applications in flexible devices due to their mechanical and electrical properties and the effect of their bulk and interfacial properties on overall behavior.[11−17,26] Accordingly, graphenes, which are composed of carbon atoms arranged in a honeycomb lattice, are expected to be potential building blocks of flexible SCs because of their remarkable electrical and mechanical properties.[13,14] Graphene, chemically modified graphene, and graphene-based composites have been used as electrode materials for high-performance SCs as previously reported.[27−29] However, the bulk size and wet system of such a cell configuration has not been shown to be suitable for all-solid-state and flexible energy-storage devices, and no test of performance durability under mechanical stress has been performed. In full consideration of these problems, both highly conductive robust thin films and their easy assembly techniques of electrode and solid electrolyte are demonstrated here to realize highly flexible and all-solid-state SCs.

* Address correspondence to hammond@mit.edu (P.T.H.), phs0727@khu.ac.kr (H.S.P.).

Received for review June 1, 2011 and accepted August 8, 2011.

**Published online August 08, 2011**
10.1021/nn202020w

Fast ionic transport at the electrochemical interfaces is critical for effective energy storage in SCs.[30,31] In particular, the physical energy storage of EDLCs is determined by the ion diffusion and accumulation on the surface of the electrode at the electrode/electrolyte interface through a nonfaradaic process.[18] A comprehensive investigation into the kinetics of ions at the interface has been carried out for the development of high-performance SCs: the ion diffusion into micropores of activated carbon,[32−34] the surface adsorption of ions on carbon nanotubes (CNT),[35,36] and the facilitated ion diffusion into the wetted carbon surface.[37,38] At the microscopic level, the interaction of lithium ion with single- and few-layer graphenes was experimentally studied, and the lithium ion diffusion in graphene was theoretically investigated for lithium-ion batteries.[39] Despite these intensive efforts for the theoretical and experimental analyses on the ion movement at the interface, the fundamental understanding of the ion diffusion into macroscopic graphene-based electrodes and even of the electrochemical behavior in all-solid-state SCs is still unexplored.

Herein we demonstrated all-solid-state flexible SCs prepared through the assembly of Nafion-functionalized reduced graphene oxide (f-RGO) thin films (as electrode) and solvent-cast Nafion electrolyte membranes (as electrolyte and separator). The superiority of all-solid-state flexible f-RGO SCs was demonstrated by the 2-fold higher capacitance and rate capability compared to those of all-solid-state graphene SCs and the good performance durability under the cycles of bending and relaxing. Importantly, the facilitated charge and ion transport at the interface was comprehensively studied for the development of high-performance SC devices.

## RESULTS AND DISCUSSION

The configuration of all-solid-state flexible thin SCs described herein is schematically shown in Figure 1a. Considering that the major components of SCs are electrode, separator, and electrolyte, the key procedures to configure these simple SCs are the fabrication of functionalized graphenes, their assembly into flexible thin films, and the integration of the three components. For the fabrication of Nafion-functionalized graphenes, graphene oxides (GOs) were prepared by the Hummers method[40] and then coated by Nafion. Highly homogeneous f-RGO solutions were obtained from the reduction of the resultant Nafion-functionalized GOs. Free-standing flexible f-RGO films were readily fabricated through directional convective assembly. The f-RGO films were transferred onto polyethylene−terephthalate (PET) substrates, in which thin gold films were deposited by the electron-beam evaporation technique on the edge of each f-RGO film for electrical contact. In order to assemble the all-solid-state flexible SC devices, the as-prepared Nafion

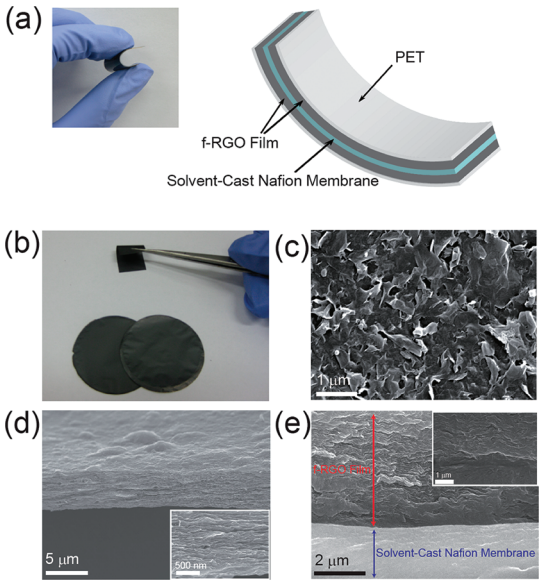


**Figure 1. (a) Photograph and schematic diagram of all-solid-state flexible thin f-RGO-SC. (b) Photograph of f-RGO films. (c) SEM image of surface on f-RGO films. (d) SEM images of cross-section of f-RGO films (inset is high-magnification SEM image). (e) SEM images of cross-section of f-RGO-SC (inset is high-magnification SEM image).**

polymer solution in *N,N*-dimethylacetamide was mixed with $H_2SO_4$, slowly poured on the f-RGO thin film, and then dried at 60 °C for 6 h. The resultant materials were used as solvent-cast Nafion electrolyte membranes. Another f-RGO film was wetted by Nafion solution and then stacked on the Nafion electrolyte membrane coated on the opposite f-RGO film. After the solidification of electrolyte, the f-RGO/Nafion membrane/f-RGO-assembled SC device in the two-electrode system was annealed at 120 °C for 6 h. The successful integration of f-RGO-SC was obtained through a hot pressing procedure, which resulted in close contact between the electrolyte and the electrode for device consolidation. The resultant all-solid-state flexible thin SCs are composed of f-RGOs with a thickness of 5 $\mu$m as electrode and a solid Nafion membrane with a thickness of 20 $\mu$m as both electrolyte and separator. The detailed information for the fabrication of RGOs, f-RGOs, f-RGO films, and flexible SCs is provided in the Experimental Section.

In the present work, the utilization of Nafion polymer is of significant importance in terms of the rational design and fabrication of the conductive and robust electrode materials and the tight integration of electrodes and electrolytes to improve the interfacial characteristics for high-performance flexible SCs. Nafion can easily functionalize carbon nanomaterials because of its intrinsic structure, which is composed of mainly two parts: $-CF_2$ groups making a hydrophobic backbone and $-SO_3^-$ groups making hydrophilic side chains.[41] For instance, it was demonstrated that the strong interactions between the Nafion and the CNTs result in highly homogeneous hybrid solutions.[42]

Similarly, RGOs can be functionalized with Nafion polymer based on supramolecular assembly. The f-RGOs were synthesized by chemical reduction of GOs previously functionalized with Nafion polymer through the mutual hydrophobic and hydrophilic interactions between both amphiphilic features of GOs and Nafion. The chemical characterization of f-RGOs was provided in the Supporting Information. The f-RGO solutions exhibited enhanced processability and then created shiny and flexible f-RGO films without any cracks through a directional convective assembly as shown in Figure 1b. Scanning electron microscopy (SEM) images show that the surfaces of the f-RGO films are wrinkled and curved (Figure 1c), while their cross-sections are highly packed and interlocked with a layered arrangement of the isolated nanosheets (Figure 1d). The favorable interfacial contact between the f-RGO films and Nafion membrane was achieved by the infiltration of Nafion electrolyte into the pores of f-RGO films during the solvent casting of the Nafion membrane (Figure 1e). In an analogous manner to GO or graphene papers as reported previously,[43−45] f-RGO films had well-defined macroscopic structures, the so-called interconnecting network structures, which can induce good mechanical properties of composite films by means of the compactly interlocked morphology and high electrical properties attributable to the percolated, fast charge transfer. In addition, the rough and porous structures of the film surfaces can improve the capacitance by increasing the accessible specific area at the electrolyte/electrode interface.[46,47] Consequently, these complementary inner and surface structures of f-RGO films are thought to become a proper electrode for high-performance flexible SCs.

Both good electrical and good mechanical properties of electrodes are prerequisites for the implementation of flexible thin SC devices.[11−17] The RGO-based supercapacitors (RGO-SCs), prepared by experimental procedures identical to that of the f-RGO-based supercapacitors (f-RGO-SCs), were used as a control in order to demonstrate the superiority of f-RGO-SCs. The mechanical and electrical properties of f-RGO films were analyzed by varying the weight ratio of Nafion loading relative to GOs (0:100, 2:98, 5:95, 10:90, 15:85, 30:70, 50:50, and 70:30 wt %), as shown in Figure 2. The typical stress−strain plots indicate that f-RGO films with >5 wt % loading of Nafion showed higher mechanical properties, 30.1 GPa of Young's modulus and 170.2 MPa for tensile strength, compared to those values for the RGO films: 22.2 GPa for Young's modulus and 105.5 MPa for tensile strength. The mechanical properties of f-RGO films were enhanced with respect to the content of Nafion in these experimental conditions. In contrast, the electrical conductivity of f-RGO films was gradually reduced at the low Nafion loading and rapidly dropped at 15 wt % of Nafion loading. On the basis of the

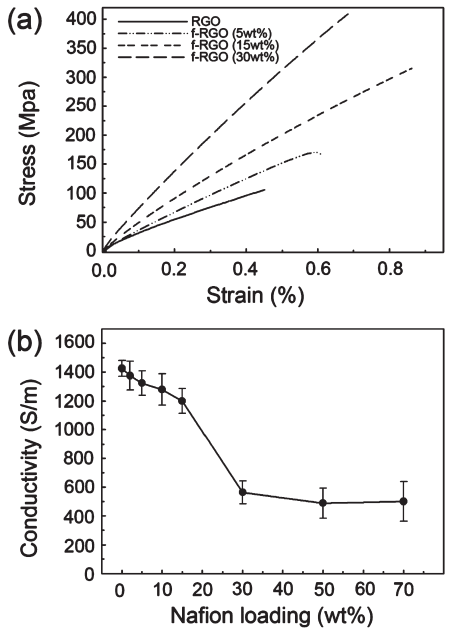


**Figure 2. (a) Stress−strain curves of RGO film and f-RGO films (Nafion loading: 5, 15, and 30 wt %) and (b) electrical conductivities of f-RGO films with respect to the loading of the Nafion from left: 0, 2, 5, 10, 15, 30, 50, and 70 wt %.**

mechanical and electrical properties, the f-RGO-SCs with 5 wt % of Nafion loading were chosen to compare to RGO-SCs, and the specific capacitances of f-RGO-SCs in the Nafion loading range between 5 and 30 wt % were also given to optimize the chemical compositions (see Figure S1). Consequently, the f-RGO films with 5 wt % of Nafion loading are suitable for the concept of flexible SCs because they meet the requirements of high mechanical and good electrical properties. Despite the lower conductivity of f-RGO films compared to that of a pristine RGO film, furthermore, the former had better capacitance due to the facilitated charge propagation and ion diffusion at the electrolyte/electrode interface and higher mechanical stability because of the durable film consolidation (detailed discussion will be provided below).

The electrochemical behavior and capacitor performances of RGO-SC and f-RGO-SC devices with the two-electrode system were analyzed by galvanostatic charge/discharge, cyclic voltammetry (CV), and impedance measurements. For the CV curves, the specific capacitance (*C*) values were calculated by dividing the current by the voltage scan rate for two electrodes.[27] In comparison with the CV results of RGO-SCs, the f-RGO-SCs displayed more rectangular-shaped profiles, which can be attributed to ideal capacitive behavior as a consequence of the fast charge and ion transport (see Figure S2). At the scan rate of 50 mV/s the f-RGO-SCs obtained 124.2 F/g, a 2-fold higher value compared to 64.2 F/g for RGO-SCs. This finding was confirmed by the galvanostatic charge/discharge curves of f-RGO-SCs and RGO-SCs at 1 A/g current density (Figure 3a).

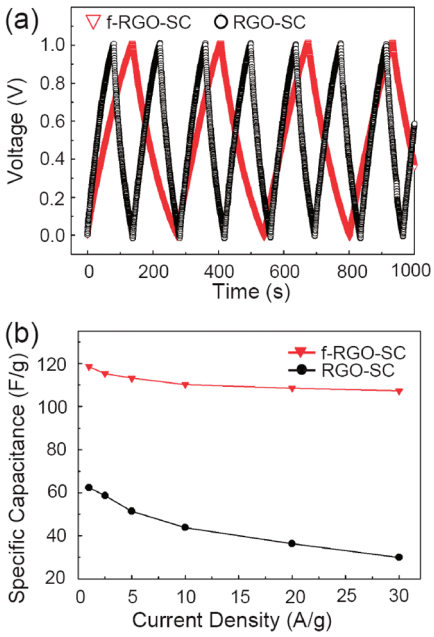


**Figure 3. (a) Charge−discharge cycles measured with a constant current density of 1 A/g for RGO-SC and f-RGO-SC and (b) specific capacitances of RGO-SC and f-RGO-SC at different constant current densities: 1, 2.5, 5, 10, 20, and 30 A/g.**

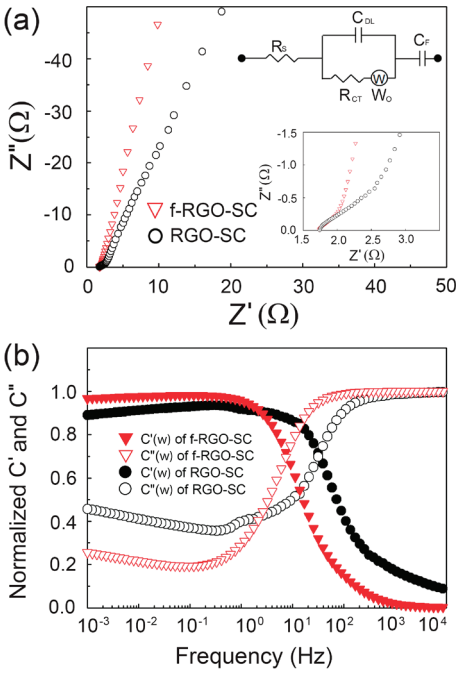


**Figure 4. (a) Nyquist plots of RGO-SC and f-RGO-SC (insets are the magnified view of the Nyquist curves and equivalent circuit) and (b) normalized real and imaginary part capacitances of RGO-SC and f-RGO-SC as a function of frequency.**

In the case of galvanostatic charge/discharge, the $C$ value was calculated by following eq 1:[28]

$$C = I/[m(\Delta V/\Delta t)] \quad (1)$$

where $I$ is the current applied, $\Delta V/\Delta t$ is the slope of the discharge curve after the $IR$ drop, and $m$ is the mass of the f-RGO electrodes. Obviously, the specific capacitance of f-RGO-SC of 118.5 F/g is about 2-fold higher than the 62.3 F/g of the RGO-SC, and the results of f-RGO-SCs and RGO-SCs obtained from galvanostatic cycling were consistent with those of CV. In the range of current density from 1 to 30 A/g, the specific capacitances of f-RCO-SCs are ~2−3 times higher than those of RGO-SCs (Figure 3b). In particular, the capacitance values of f-RGO-SCs remained almost constant (90% retention at 30 A/g) with respect to the changes in the current densities from 1 to 30 A/g, while those of RGO-SCs were dramatically decreased (48% retention at 30 A/g). In the case of the variation of scan rate, the f-RGO-SCs and RGO-SCs also showed the same capacitance behavior as the variation of current densities (see Figure S3). This finding indicates the higher rate capability of f-RGO-SCs compared to that of RGO-SCs. Considering that the electrical conductivity of the RGO electrode was higher than that of the f-RGO and that the identical electrolyte, Nafion membrane, was used for the two SCs, the capacitance performances are thought to be dominantly influenced by the interfacial characteristics such as ion diffusion, charge transfer resistance, and charge propagation at the electrode/electrolyte interface rather than by intrinsic bulk electronic and ionic conductivities of the electrode and electrolyte, respectively.

Electrochemical impedance spectroscopy (EIS) is a very powerful tool for fundamentally understanding the electrochemical behaviors of RGO-SCs and f-RGO-SCs at the bulk and interface in terms of the equivalent circuit models consisting of resistive and capacitive elements.[33−36] Figure 4a shows the Nyquist plots of RGO-SCs and f-RGO-SCs in the frequency range of 10 kHz to 10 mHz measured at an equilibrium open circuit potential of 10 mV. The Nyquist plot was well-fit to an equivalent circuit as shown in the inset of Figure 4a by following eq 2:[36]

$$Z = R_S + \frac{1}{jwC_{DL} + \frac{1}{R_{CT} + W_o}} - j\frac{1}{wC_F} \quad (2)$$

where $R_S$ is bulk resistance, $C_{DL}$ is double-layer capacitance, $W_o$ is the finite-length Warburg diffusion element, $R_{CT}$ is charge transfer resistance, and $C_F$ is the faradic capacitance. The typical Nyquist spectra of SCs can be classified into three regions following the frequency level. At high frequency, the intersection point on the real axis represents the ohmic resistance of the electrolyte and the internal resistance of the electrode, which is described as $R_S$. The semicircular behavior in the high- to midfrequency region corresponds to the parallel connection of the interfacial charge transfer resistance, $R_{CT}$, and the double-layer capacitance, $C_{DL}$. The transition from the semicircle

to the long tail is attributed to the ion diffusion inside the electrode, resulting in the Warburg element, $W_o$, which is expressed as $A/(j\omega)^n$, where $A$ is called the Warburg coefficient, $\omega$ is the angular frequency, and $n$ is an exponent. At low frequency, a straight line parallel to the imaginary axis is derived from an ideally polarizable capacitance: the incline to the real axis is due to the resistive element of the nonideal capacitance. Table 1 shows $R_S$, $R_{CT}$, $C_{DL}$, $C_F$, and $W_o$ of RGO-SCs and f-RGO-SCs. The $R_S$ and $R_{CT}$ of RGO-SCs are 1.50 and 1.12 Ω, while those of f-RGO-SCs are 1.70 and 0.27 Ω, respectively. The slight increase in the $R_S$ and the decrease of $R_{CT}$ of f-RGO due to the functionalization of Nafion polymer indicate that the interfacial characteristics strongly improved the performances of SCs based on graphene. The higher Warburg slope of the f-RGO-SCs compared to that of the RGO-SCs is indicative of the faster ion movement for the formation of the electrical double layer. The influence of Nafion polymer on the capacitance performance of the SCs was further studied by the Bode plots (see Figure S4). The phase angle value of f-RGO-SCs at −76° is closer to that of an ideal capacitor at −90°,[48] compared to that of RGO-SCs at −62°. These results indicate that the f-RGO-SCs show an enhanced charge transfer due to the favorable interface of the electrode and the electrolyte.

An alternative approach to the impedance analysis of SCs is to directly consider them as a whole by using the impedance data. The complex form of capacitance dependent on frequency, or $C(w)$, is defined by eqs 3 and 4:[33]

$$C(w) = C'(w) - iC''(w) \quad (3)$$

$$C'(w) = \frac{-Z''(w)}{w|Z(w)|^2},\ C''(w) = \frac{Z'(w)}{w|Z(w)|^2} \quad (4)$$

where $C'(w)$ and $C''(w)$ are the real and imaginary part of the capacitance, $C(w)$, respectively.

The low frequency value of $C'(w)$, which corresponds to the capacitance of the cell measured from the galvanostatic charge−dischrge, is characteristic of the electrode structure and the electrode/electrolyte interface. In contrast, $C''(w)$ is ascribed to the energy dissipation by an irreversible process. Consequently, SCs, especially in EDLCs, oscillate between two states such as resistance at high frequency and capacitance at low frequency. In particular, a time constant defined as $\tau_0 = 1/f_0$, which is known as a dielectric relaxation time characteristic of the whole system, is obtained from the maximum $C''(w)$ at frequency $f_0$.[33] The RGO-SCs and f-RGO-SCs had a relaxation time of 0.87 and 0.17 s, respectively, in these measurement conditions. In order to demonstrate the contribution of these two states to the capacitance, both $C'(w)$ and $C''(w)$ are normalized to $|C(w)|$, as shown in Figure 4b. The f-RGO-SCs clearly exhibited more capacitive and less resistive behavior, compared to the RGO-SCs, at the low-frequency range where the ion diffusion occurs. Therefore, the facilitated ion diffusion at the electrical double layer is proven by the 4-fold faster relaxation of the f-RGO-SCs than that of the RGO-SCs and more capacitive behavior of the former at the low-frequency region, which emphasizes the merits of the f-RGO-SC system.

**TABLE 1. Components of the Equivalent Circuit Fitted for the Impedance Spectra Shown in Figure 4a**

| | | | | $W_o = A/(j\omega)^n$ | | |
|---|---|---|---|---|---|---|
| | $R_S$ (Ω) | $R_{CT}$ (Ω) | $C_{DL}$ (mF/g) | $A(\Omega \cdot s^{-n})$ | $n$ | $C_F$ (F/g) |
| RGO-SC | 1.5 | 1.21 | 1.8 | 13 | 0.56 | 59 |
| f-RGO-SC | 1.7 | 0.27 | 2.1 | 31 | 0.63 | 102 |

Herein, it is possible to demonstrate the improvement of ion and charge transport at the interface as a consequence of the functionalization by Nafion polymer along four main lines of thought. First, the charge propagation of f-RGO-SCs, especially in ion transfer, as demonstrated by the rectangular CV behavior, $R_{CT}$, and Warburg slope, was facilitated by the high ionic conductivity of Nafion polymer coated on RGOs. Ions can readily accumulate on the surface of the electrode by means of fast ion mobility for the boosted charge propagation. Second, the wetting behavior of Nafion polymer makes mobile ions easily accessible to the pores of f-RGOs. The easy access to the pores of f-RGOs is important to increase the performance of EDLCs by means of low mass transfer resistance of ions at the interface, because the capacitance is dependent on the density of charges physically adsorbed on the surface of the pores at the electrical double layer that consists of Stern and diffuse layers, as suggested by the Stern model.[18] Third, Nafion polymer acted as an electrochemical binder for the adhesion of the Nafion-coated electrode and Nafion membrane in the process of assembly into solid-state supercapacitors.[49,50] The lower $R_{CT}$ of f-RGO compared to that of RGO can be the result of the close contact between the electrode and the electrolyte due to the role of Nafion polymer as a binder, which was assisted by hot pressing. Fourth, the interconnected networks of f-RGO are beneficial for the percolating systems of charge transfer in terms of the construction of continuous transport pathways, which boost the fast charge transport. A homogeneous interdistribution of Nafion polymer/graphene in hybrid systems makes the diffusion path of ion species shorter.

The performance durability of f-RGO-SCs under cyclic strains should be addressed to demonstrate the potential for flexible energy-storage devices as shown in Figure 5. The capacitance performances of f-RGO-SCs at 100 mV/s of scan rate were measured with

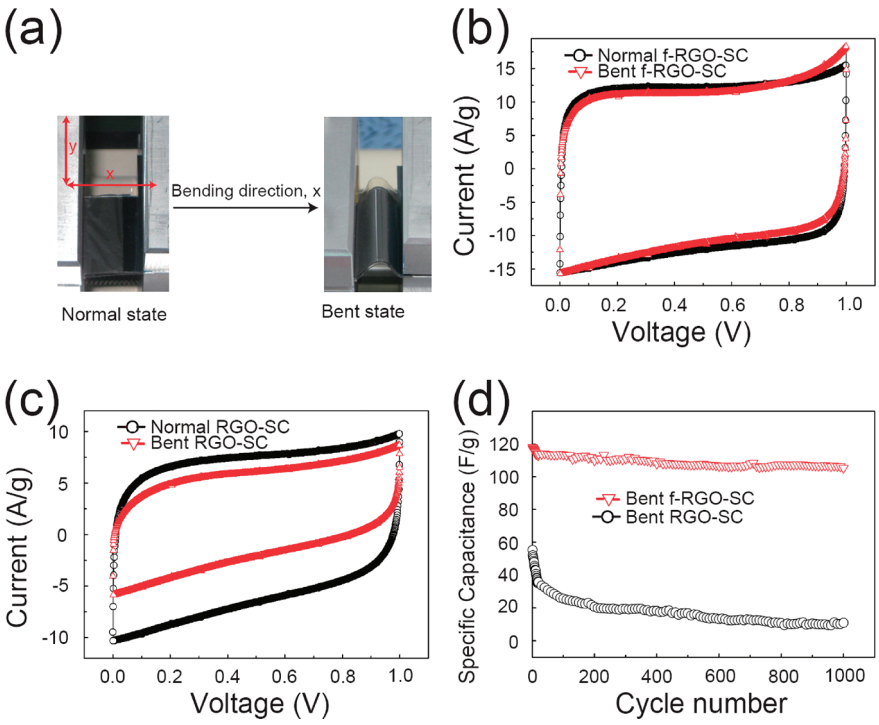


**Figure 5. (a) Photographs of SC prior to the bent experiments, (b) cyclic voltammograms of f-RGO-SC and bent f-RGO-SC at 100 mV/s scan rate, (c) cyclic voltammograms of RGO-SC and bent RGO-SC at 100 mV/s scan rate, and (d) durability test of RGO-SC and f-RGO-SC by measuring 1000 charge–discharge cycles with a constant current density of 1 A/g at the bent state.**

respect to a bending radius of 2.2 mm, corresponding to −28.5% of the maximum applied tensile strain, while those of RGO-SCs were tested as a control under identical conditions. In comparison to the previous results under no strain, the CV curves of the f-RGO-SCs displayed almost the same rectangular shape and specific capacitances as those before the bending test. In contrast, the bending tests changed the CV curves of the RGO-SCs into nonrectangular shapes, and their specific capacitances were reduced from 68 F/g to 40 F/g. In order to confirm the performance durability of the f-RGO-SCs, galvanostatic charge–discharge tests at the constant current density of 1 A/g up to 1000 cycles were carried out with the bending of devices to −28.5% tensile strain. Remarkably, no significant changes in the specific capacitances of f-RGO-SCs were observed during 1000 charge–discharge cycles, whereas those of RGO-SCs dramatically decreased with the cycling of bending. Even during severe bending and long-term cycling tests, the specific capacitances of the f-RGO-SCs remained stable. It is worthwhile to note that the interpenetrating networking structures of the f-RGO and the good adhesion between electrode and electrolyte led to the mechanical integrity of the consolidated films as well as to the favorable interfacial electrochemical behaviors.

## CONCLUSION

We have demonstrated a general and rational strategy to fabricate all-solid-state flexible thin SCs through the integration of robust, conductive, and free-standing f-RGO electrodes and a solid Nafion electrolyte under the hot pressing procedure. Notably, the f-RGO-SCs revealed high specific capacitance and rate capability due to the fast ion and charge transport at the interface, as well as no noticeable decrease in performance over long device operating times under bending conditions as a result of good mechanical integrity. In particular, the facilitated ion diffusion and charge transfer in SCs was intensively studied to understand the improvement of performance by means of the functionalization of RGO by Nafion polymer. Therefore, this concept would pave a simple and useful way to the development of all-solid-state flexible energy-storage devices, allowing for the fundamental understanding of electrochemical behavior at the interface.

## EXPERIMENTAL SECTION

**Chemicals.** Graphite powder (<20 $\mu$M), hydrazine solution (35 wt % in water), and Nafion (perfluorinated resin solution, 5 wt % in lower aliphatic alcohol and water mixture) were purchased from Aldrich. 1-Propanol was obtained from Junsei.

**Synthesis of f-RGO.** GOs as raw materials were synthesized by the modification of Hummers method and described elsewhere.[40] Prior to the preparation of f-RGO, dry GOs

(10 mg) were fully exfoliated in deionized (DI) water (10 mL) by ultrasonic treatment for 30 min (Fisher Scientific model 500 ultrasonic, 350 W), and then 1-propanol (10 mL) solution was added into the GOs in DI water. The complete exfoliation of GOs in DI water/1-propanol solvent was confirmed by TEM and AFM analyses as shown in Figure S5. In order to functionalize RGOs with Nafion polymer, varying the weight ratio of Nafion loading relative to GOs (0:100, 2:98, 5:95, 10:90, 15:85, 30:70, 50:50, and 70:30 wt %), they were mixed with 0.5 mg/mL of GOs in 20 mL of DI water/1-propanol bisolvents (volume ratio of 50:50). The mixture of GOs and Nafion was treated by sonication for 60 min. A highly homogeneous black dispersion of f-RGOs was obtained after reduction was achieved by addition of 100 $\mu$L of hydrazine solution at 85 °C for 24 h. The resulting mixture was washed with DI water and ethanol several times, and the f-RGOs were purified by dialysis for one week to remove the remaining hydrazine and impurities. Finally, the powder was filtered and dried under vacuum at room temperature and stored. Characterization of chemical structures of f-RGOs was performed by the analysis of FT-IR, XPS, NMR, and Raman spectroscopies as show in Figures S6−S10.

**Fabrication of f-RGO-SC Devices.** The f-RGO-SCs were prepared by assembly of a solvent-cast Nafion electrolyte membrane with two f-RGO films face-to face. Prior to fabricating the SC devices, the f-RGO films were prepared by filtering homogeneous solutions in DI water/1-propaonl (volume ratio of 50:50) bisolvents through an Anodisc membrane filter (47 mm in diameter, 0.2 $\mu$m pore size, Whatman). The resulting films were dried in air and peeled off of the filter membrane, reported in the method for preparation of GO papers. As-prepared free-standing flexible conductive f-RGO films served as electrodes for SCs. The f-RGO films were transferred onto polyethylence-terephthalate (PET) substrates, where thin gold films were deposited on the edge of each f-RGO film for electrical contact by the electron-beam evaporation technique. On the other hand, in order to integrate all-solid-state flexible thin SCs, a Nafion membrane was used as both electrolyte and separator and prepared following the procedure. Nafion solution in *N*,*N*-dimethylacetamide was mixed with $H_2SO_4$ (50 wt %) and then was stirred until the mixture became a homogeneous solution. In order to assemble into all-solid-state flexible SC devices, the as-prepared Nafion solution was slowly poured on the f-RGO thin film and then dried at 60 °C for 6 h. Another f-RGO film was wetted by Nafion solution and then stacked on the Nafion electrolyte coated on f-RGO film. After the solidification of the electrolyte, the f-RGO/Nafion membrane/f-RGO-assembled SC device was annealed at 120 °C for 6 h. The successful integration of f-RGO-SC was obtained through a hot pressing procedure at 100 kg/cm$^2$ and 130 °C for 3 min, which resulted in close contact between the electrolyte and the electrode for device consolidation. The resultant SC devices were immersed in a 1 M $H_2SO_4$ solution and dried at 60 °C prior to use. All-solid-state flexible thin SCs are composed of f-RGOs with a thickness of 5 $\mu$m as electrode and solid Nafion membrane with a thickness of 20 $\mu$m as both electrolyte and separator. RGO-SCs as a control sample were prepared following the same protocols as RGO-SCs.

**Characterization.** Transmission electron microscopy (TEM) images were collected on an E.M. 912 Ω energy-filtering TEM (EF TEM 120 kV) and a JEM-3010 HR TEM (300 kV). The scanning electron microscopy (SEM) micrographs were obtained using a field emission scanning electron microscope (FEI Sirion model) equipped with an in-house Schottky emitter in high stability. The atomic force microscopy (AFM) images were recorded in the noncontact mode using a Nanoman Digital Instruments 3100 AFM (VEECO) with an etched silicon aluminum coated tip. The Fourier transform infrared (FT-IR) spectra were collected on a JASCO FT-IR 470 plus. Each spectrum was recorded from 4000 to 650 cm$^{-1}$ with using 12 scans at a resolution of 4 cm$^{-1}$. The diffraction angle of the diffractograms was in the range $2\theta$ = 5−40°. Solid-state magic angle spinning (MAS) nuclear magnetic resonance (NMR) spectra were collected on a Bruker Avance 400 spectrometer operating at 10 kHz using a 4 mm MAS. Spectra based on free induction decays with moderate decoupling power were averaged over 4000 scans with a recycle delay of 4 s. The Raman spectra were recorded from 3500 to 100 cm$^{-1}$ on a Bruker FT Raman spectrophotometer RFS 100/S using a 785 and 1064 nm dual-channel laser at a resolution of 1 cm$^{-1}$. The X-ray photoelectron spectroscopy (XPS) data were obtained using a Thermo MultiLab 2000 system. An Al Mgα X-ray source at 200 W was used with pass energy of 20 eV and 45° takeoff angle under $10^{-7}$ Torr vacuum analysis chamber. The high-resolution scans of C and low-resolution survey scans were analyzed for each sample at least two separate locations. Electrical conductivities of RGO and f-RGO films were measured by using the standard four-point probe technique (Loresta-GP, Mitsubishi Chemical). All electrochemical data were obtained at room temperature within the error range of ±5%. Mechanical property tests were performed by a dynamic mechanical analyzer (DMA Q800, TA Instruments) at room temperature. The samples were cut with a razor blade into rectangular strips of approximately 3 × 15 mm$^2$ for mechanical testing and were gripped using film tension clamps with a clamp compliance of 0.2 $\mu$m N$^{-1}$. All tensile tests were conducted in controlled strain rate mode with a preload of 0.01 N and a strain ramp rate of 0.05%/min. Tensile modulus was determined by fitting the stress−strain plot in the elastic regime with a straight line. The electrochemical characteristics were evaluated by cyclic voltammetry using a CHI 760D electrochemical workstation (CH Instruments) and galvanostatic charge/discharge using a Solartron 1260 at room temperature (RT). CV measurements were performed at different voltage scan rates in a range from 10 to 500 mV/s. Galvanostatic charge/discharge measurements were carried out at different current density from 1 to 30 A/g. The electrochemical impedance spectroscopy measurements were performed over a frequency range from $10^6$ to $10^{-3}$ Hz at the amplitude of the sinusoidal voltage of 10 mV and RT on supercapacitor devices using a Solartron 1260 impedance/gain-phase analyzer. The performance of flexible SCs was demonstrated by measuring the capacitance of SCs with respect to a radius of 2.2 mm, corresponding to −28.5% of the applied tensile strain. A life cycling test of SCs was taken by measuring the galvanostatic charge/discharge at the constant current density of 1 A/g up to 1000 cycles with the bending of devices to −28.5% of the applied tensile strain (2.2 mm of bending radius).

*Acknowledgment.* This research was supported by both Basic Science Research Program through the National Research Foundation of Korea (NRF) funded by the Ministry of Education, Science and Technology (2011-0007677) and a grant from the Fundamental R&D Program for Core Technology of Materials funded by the Ministry of Knowledge Economy.

*Supporting Information Available:* CV curves of f-RGO-SCs as a function of Nafion loadings; comparison of CV curves for RGO-SC and f-RGO-SC devices; CV curves of RGO-SC and f-RGO-SC at various scan rates in order to investigate rate capability; Bode plots of RGO-SC and f-RGO-SC; TEM and AFM images of GO; FT-IR, survey XPS, C1s XPS, solid-state $^{13}$C MAS NMR, and Raman spectra of GO, RGO, and f-RGO. This material is available free of charge *via* the Internet at http://pubs.acs.org.

## REFERENCES AND NOTES

1. Ju, S.; Facchetti, A.; Xuan, Y.; Liu, J.; Ishikawa, F.; Ye, P.; Zhou, C.; Marks, T. J.; Janes, D. B. Fabrication of Fully Transparent Nanowire Transistors for Transparent and Flexible Electronics. *Nat. Nanotechnol.* **2007**, *2*, 378–384.
2. Kim, D.-H.; Ahn, J.-H.; Choi, W. M.; Kim, H.-S.; Kim, T.-H.; Song, J.; Huang, Y. Y.; Liu, Z.; Lu, C.; Rogers, J. A. Stretchable and Foldable Silicon Integrated Circuits. *Science* **2008**, *320*, 507–511.
3. Sun, Y.; Choi, W. M.; Jiang, H.; Huang, Y. Y.; Rogers, J. A. Controlled Buckling of Semiconductor Nanoribbons for Stretchable Electronics. *Nat. Nanotechnol.* **2006**, *1*, 201–207.
4. Ahn, B. Y.; Duoss, E. B.; Motala, M. J.; Guo, X.; Park, S.-I.; Xiong, Y.; Yoon, J.; Nuzzo, R. G.; Rogers, J. A.; Lewis, J. A. Omnidirectional Printing of Flexible, Stretchable, and Spanning Silver Microelectrodes. *Science* **2009**, *323*, 1590–1593.

5. Cao, Q.; Kim, H.-S.; Pimparkar, N.; Kulkarni, J. P.; Wang, C.; Shim, M.; Roy, K.; Alam, M. A.; Rogers, J. A. Medium-Scale Carbon Nanotube Thin-Film Integrated Circuits on Flexible Plastics Substrates. *Nature* **2008**, *454*, 495–500.
6. Kim, D.-H.; Song, J.; Choi, W. M.; Kim, H.-S.; Kim, R.-H.; Liu, Z.; Huang, Y. Y.; Hwang, K.-C.; Zhang, Y.-W.; Rogers, J. A. Materials and Noncoplanar Mesh Designs for Integrated Circuits with Linear Elastic Responses to Extreme Mechanical Deformations. *Proc. Natl. Acad. Sci. U. S. A.* **2008**, *105*, 18675–18680.
7. Sekitani, T.; Nakajima, H.; Maeda, H.; Fukushima, T.; Aida, T.; Hata, K.; Someya, T. Stretchable Active-Matrix Organic Light-Emitting Diode Display Using Printable Elastic Conductors. *Nat. Mater.* **2009**, *8*, 494–499.
8. Ko, H. C.; Stoykovich, M. P.; Song, J.; Malyarchuk, V.; Choi, W. M.; Yu, C.-J.; Geddes, J. B., III; Xiao, J.; Wang, S.; Huang, Y.; *et al*. A Hemispherical Electronic Eye Camera Based on Compressible Silicon Optoelectronics. *Nature* **2008**, *454*, 748–753.
9. Kim, K. S.; Zhao, Y.; Jang, H.; Lee, S. Y.; Kim, J. M.; Kim, K. S.; Ahn, J.-H.; Kim, P.; Choi, J.-Y.; Hong, B. H. Large-Scale Pattern Growth of Graphene Films for Stretchable Transparent Electrodes. *Nature* **2009**, *457*, 706–710.
10. Sekitani, T.; Noguchi, Y.; Hata, K.; Fukushima, T.; Aida, T.; Someya, T. A Rubberlike Stretchable Active Matrix Using Elastic Conductors. *Science* **2008**, *321*, 1468–1472.
11. Hu, L.; Pasta, M.; Mantia, F. L.; Cui, L.; Jeong, S.; Deshazer, H. D.; Choi, J. W.; Han, S. M.; Cui, Y. Stretchable, Porous, and Conductive Energy Textiles. *Nano Lett.* **2010**, *10*, 708–714.
12. Meng, C.; Liu, C.; Chen, L.; Hu, C.; Fan, S. Highly Flexible and All-Solid-State Paperlike Polymer Supercapacitors. *Nano Lett.* **2010**, *10*, 4025–4031.
13. Wu, Q.; Xu, Y.; Yao, Z.; Liu, A.; Shi, G. Supercapacitors Based on Flexible Graphene/Polyaniline Nanofiber Composite Films. *ACS Nano* **2010**, *4*, 1963–1970.
14. Wang, D.-W.; Li, F.; Zhao, J.; Ren, W.; Chen, Z.-G.; Tan, J.; Wu, Z.-S.; Gentle, I.; Lu, G. Q.; Cheng, H.-M. Fabrication of Graphene/Polyaniline Composite Paper *via In Situ* Anodic Electropolymerization for High-Performance Flexible Electrode. *ACS Nano* **2009**, *3*, 1745–1752.
15. Pushparaj, V. L.; Shaijumon, M. M.; Kumar, A.; Murugesan, S.; Ci, L.; Vajtai, R.; Linhardt, R. J.; Nalamasu, O.; Ajayan, P. M. Flexible Energy Storage Devices Based on Nanocomposite Paper. *Proc. Natl. Acad. Sci. U. S. A.* **2007**, *104*, 13574–13577.
16. Kaempgen, M.; Chan, C. K.; Ma, J.; Cui, Y.; Gruner, G. Printable Thin Film Supercapacitors Using Single-Walled Carbon Nanotubes. *Nano Lett.* **2009**, *9*, 1872–1876.
17. Hiralal, P.; Imaizumi, S.; Unalan, H. E.; Matsumoto, H.; Minagawa, M.; Rouvala, M.; Tanioka, A.; Amaratunga, A. J. Nanomaterial-Enhanced All-Solid Flexible Zinc-Carbon Batteries. *ACS Nano* **2010**, *4*, 2730–2734.
18. Simon, P.; Gogotsi, Y. Materials for Electrochemical Capacitors. *Nat. Mater.* **2008**, *7*, 845–854.
19. Zhang, L. L.; Zhou, R.; Zhao, X. S. Graphene-Based Materials as Supercapacitor Electrodes. *J. Mater. Chem.* **2010**, *20*, 5983–5992.
20. Zhang, L. L.; Zhao, X. S. Carbon-based Materials as Supercapacitor Electrodes. *Chem. Soc. Rev.* **2009**, *38*, 2520–2531.
21. Yuan, C. Z.; Gao, B.; Shen, L. F.; Yang, S. D.; Hao, L.; Lu, X. J.; Zhang, F.; Zhang, L. J.; Zhang, X. G. Hierarchically Structured Carbon-based Composites: Design, Synthesis and Their Application in Electrochemical Capacitors. *Nanoscale* **2011**, *3*, 529–545.
22. Winter, M.; Brodd, R. J. What Are Batteries, Fuel Cells, and Supercapacitors?. *Chem. Rev.* **2004**, *104*, 4245–4270.
23. Fan, L.-Z.; Hu, Y.-S.; Maier, J.; Adelhelm, P.; Smarsly, B.; Antonietti, M. High Electroactivity of Polyaniline in Supercapacitors by Using a Hierarchically Porous Carbon Monolith as a Support. *Adv. Funct. Mater.* **2007**, *17*, 3083–3087.
24. Portet, C.; Lillo-Ródenas, M. Á.; Linares-Solano, A.; Gogotsi, Y. Capacitance of KOH Activated Carbide-Derived Carbons. *Phys. Chem. Chem. Phys.* **2009**, *11*, 4943–4945.
25. Zhao, L.; Fan, L.-Z.; Zhou, M.-Q.; Guan, H.; Qiao, S.; Antonietti, M.; Titirici, M.-M. Nitrogen-Containing Hydrothermal Carbons with Superior Performance in Supercapacitors. *Adv. Mater.* **2010**, *22*, 5202–5206.
26. Qi, Y.; McAlpine, C. Nanotechnology-enabled Flexible and Biocompatible Energy Harvesting. *Energy Environ. Sci.* **2010**, *3*, 1275–1285.
27. Stoller, M. D.; Park, S.; Zhu, Y.; An, J.; Ruoff, R. S. Graphene-Based Ultracapacitors. *Nano Lett.* **2008**, *8*, 3498–3502.
28. Kim, T. Y.; Lee, H. W.; Stoller, M.; Dreyer, D. R.; Bielawski, C. W.; Ruoff, R. S.; Suh, K. S. High-Performance Supercapacitors Based on Poly(ionic liquid)-Modified Graphene Electrodes. *ACS Nano* **2011**, *5*, 436–442.
29. Zhu, Y.; Murali, S.; Stoller, M. D.; Ganesh, K. J.; Cai, W.; Ferreira, P. J.; Pirkle, A.; Wallace, R. M.; Cychosz, K. A.; Thommes, M.; *et al*. Carbon-Based Supercapacitors Produced by Activation of Graphene. *Science* **2011**, *332*, 1537–1541.
30. Maier, J. Nanoionics: Ion Transport and Electrochemical Storage in Confined Systems. *Nat. Mater.* **2005**, *4*, 805–815.
31. Aricò, A. S.; Bruce, P.; Scrosati, B.; Tarascon, J.-M.; Schalkwijk, W. V. Nanostructured Materials for Advanced Energy Conversion and Storage Devices. *Nat. Mater.* **2005**, *4*, 366–377.
32. Shi, H. Activated Carbons and Double Layer Capacitance. *Electrochim. Acta* **1996**, *41*, 1633–1639.
33. Taberna, P. L.; Simon, P.; Fauvarque, J. F. Electrochemical Characteristics and Impedance Spectroscopy Studies of Carbon-Carbon Supercapacitors. *J. Electrochem. Soc.* **2003**, *150*, A292–A300.
34. Fang, B.; Binder, L. A Novel Carbon Electrode Material for Highly Improved EDLC Performance. *J. Phys. Chem. B* **2006**, *110*, 7877–7882.
35. Li, X.; Rong, J.; Wei, B. Electrochemical Behavior of Single-Walled Carbon Nanotube Supercapacitors under Compressive Stress. *ACS Nano* **2010**, *4*, 6039–6049.
36. Masarapu, C.; Zeng, H. F.; Hung, K. H.; Wei, B. Effect of Temperature on the Capacitance of Carbon Nanotube Supercpacitors. *ACS Nano* **2009**, *3*, 2199–2206.
37. Hall, P. J.; Mirzaeian, M.; Fletcher, S. I.; Sillars, F. B.; Rennie, A. J. R.; Shitta-Bey, G. O.; Wilson, G.; Cruden, A.; Carter, R. Energy Storage in Electrochemical Capacitors: Designing Functional Materials to Improve Performance. *Energy Environ. Sci.* **2010**, *3*, 1238–1251.
38. Huang, J.; Sumpter, B. G.; Meunier, V. Theoretical Model for Nanoporous Carbon Supercapacitors. *Angew. Chem., Int. Ed.* **2008**, *47*, 520–524.
39. Suzuki, T.; Hasegawa, T.; Mukai, S. R.; Tamon, H. A Theoretical Study on Storage States of Li Ions in Carbon Anodes of Li Ion Batteries Using Molecular Orbital Calculations. *Carbon* **2003**, *41*, 1933–1939.
40. Hummers, W. S.; Offeman, R. E. Preparation of Graphite Oxide. *J. Am. Chem. Soc.* **1958**, *80*, 1339.
41. Mauritz, K. A.; Moore, R. B. State of Understanding of Nafion. *Chem. Rev.* **2004**, *104*, 4535–4586.
42. Zhang, J.; Gao, L.; Sun, J.; Liu, Y.; Wang, Y.; Wang, J.; Kajiura, H.; Li, Y.; Noda, K. Dispersion of Single-Walled Carbon Nanotubes by Nafion in Water/Ethanol for Preparing Transparent Conducting Films. *J. Phys. Chem. C* **2008**, *112*, 16370–16376.
43. Choi, B. G.; Hong, J.; Park, Y. C.; Jung, D. H.; Hong, W. H.; Hammond, P. T.; Park, H. S. Innovative Polymer Nanocomposite Electrolytes: Nanoscale Manipulation of Ion Channels by Functionalized Graphenes. *ACS Nano* **2011**, *5*, 5167–5174.
44. Dikin, D. A.; Stankovich, S.; Zimney, E. J.; Piner, R. D.; Dommett, G. H. B.; Evmenenko, G.; Nguyen, S. T.; Ruoff, R. S. Preparation and Characterization of Graphene Oxide Paper. *Nature* **2007**, *448*, 457–460.
45. Choi, B. G.; Park, H.; Park, T. J.; Yang, M. H.; Kim, J. S.; Jang, S.-Y.; Heo, N. S.; Lee, S. Y.; Kong, J.; Hong, W. H. Solution Chemistry of Self-Assembled Graphene Nanohybrids for High Performance Flexible Biosnesors. *ACS Nano* **2010**, *4*, 2910–2918.
46. Liu, C.; Yu, Z.; Neff, D.; Zhamu, A.; Jang, B. Z. Graphene-Based Supercapacitor with an Ultrahigh Energy Density. *Nano Lett.* **2010**, *10*, 4863–4868.

47. Miller, J. R.; Outlaw, R. A.; Holloway, B. C. Graphene Double-Layer Capacitor with ac Line-Filtering Performance. *Science* **2010**, *329*, 1637–1639.
48. Jeong, H.-K.; Jin, M.; Ra, E. J.; Sheem, K. Y.; Han, G. H.; Arepalli, S.; Lee, Y. H. Enhanced Electric Double Layer Capacitance of Graphite Oxide Intercalated by Poly(sodium 4-styrensulfonate) with High Cycle Stability. *ACS Nano* **2010**, *4*, 1162–1166.
49. Lufrano, F.; Staiti, P. Conductivity and Capacitance Properties of a Supercapacitor Based on Nafion Electrolyte in a Nonaqueous System. *Electrochem. Solid-State Lett.* **2004**, *7*, A447–A450.
50. Lufrano, F.; Staiti, P. Performance Improvement of Nafion Based Solid State Electrochemical Supercapacitor. *Electrochim. Acta* **2004**, *49*, 2683–2689.